(p,n) Cross Sections and the Strength Functions for 3- to 5.5-MeV Protons on In and on Sn Isotopes*

C. H. Johnson and R. L. Kernell†
Oak Ridge National Laboratory, Oak Ridge, Tennessee 37830
(Received 12 January 1970)

The (p,n) reaction cross sections were measured to ±4% for 3- to 5.5-MeV protons on ^{117,119,120,122,124}Sn and on natural Sn and In. Analyses with a conventional optical-model potential were made in the energy regions where the (p,n) cross sections are nearly equal to the total absorption cross sections. These analyses show that the energy dependence in the real well is about three times greater for 5- to 10-MeV protons than it is for 10- to 61-MeV protons. The best-fit potential for 3- to 5.5-MeV protons on the Sn isotopes has a surface absorptive layer about half as thick as at 10 MeV. The In strength functions are fitted by increasing both the width and depth of the imaginary part of this potential by about 25%. The Q value for ^{120}Sn$(p,n)^{120}$Sb was found to be −3465 ± 7 keV.

I. INTRODUCTION

The optical-model potential has been used extensively in recent years to describe proton elastic scattering $d\sigma(\theta)$, polarization $P(\theta)$ and the total absorption cross section σ_{abs}. Most data relative to the model have come from measurements of $d\sigma(\theta)$ and $P(\theta)$ for energies well above the Coulomb barrier, where the detailed diffraction patterns can be investigated with relative ease [at least for $d\sigma(\theta)$]. At those energies σ_{abs} is difficult to obtain with accuracy comparable to $d\sigma(\theta)$. As a result, the reaction or absorption cross sections have played minor roles in the analyses. For example, when Satchler[1] analyzed all three types of experiments at 30 MeV, he fit only $d\sigma(\theta)$ and $P(\theta)$ and then noted that the predictions for σ_{abs} were consistent with the measurements. The situation changes as the proton energy is lowered toward the top of the barrier where the diffraction patterns begin to lose their detail. Then comparable accuracy can be achieved for σ_{abs}. Bulman and Griffith[2] demonstrated this transition nicely by their accurate (±3 to ±6%) measurements on σ_{abs} for several nuclei at 9.1 MeV. They found good agreement with the predictions from elastic-scattering data for nuclei for which the energy is still above the barrier, but not for those where the energy is at or below the barrier; in the latter cases their data should be useful for adjusting the model parameters. Finally, when the energy is reduced still further, the diffraction patterns lose all detail and leave only σ_{abs} to be measured. We report here measurements of σ_{abs} for protons well below the Coulomb barrier. A brief report was published earlier.[3]

Admittedly, the single datum σ_{abs} is meager information compared to the distributions of $d\sigma(\theta)$ and $P(\theta)$. Compensation comes from the fact that σ_{abs} is fairly easy to measure. When the proton energy is below the barrier but still a few hundred keV above the (p,n) threshold, neutron emission is the major decay mode of the compound system, so $\sigma_{p,n} \simeq \sigma_{abs}$. Measurements of (p,n) excitation functions are straightforward. These functions have simple shapes so that if they were analyzed without any reference to the higher-energy data, they might reveal few details about the model potential.[4] Such a detached approach would be out of context with the model. If, on the other hand, the excitation functions are treated in a consistent and continuous manner with the model parameters from higher energies, they contain considerable information. Perhaps one can visualize these functions as playing the leading role below the barrier while the diffraction patterns play the leading role above. In any case, the cross sections must be measured accurately if they are to show more than mere consistency with extrapolations made from higher energies.

The above statement, that under certain conditions $\sigma_{p,n}$ is nearly equal to the optical-model absorption cross section σ_{abs}, is based on the statistical theory of nuclear reactions. The foundations of this theory have been discussed by many authors; for example, by Vogt.[5] The requirement for an average over many resonances in the compound system is well satisfied in the present work, which was done with about 100-keV resolution at energies where the level spacings are about[6] 10 eV. Direct (p,n) reactions are expected to be negligible; measurements of neutron spectra have shown no evidence of direct reactions at these energies[7] or at any energy below the Coulomb barrier.[8] The conditions under which the competing proton and γ-ray emission can be neglected are discussed in the Appendix.

Although several measurements[9-16] of $\sigma_{p,n}$ for

intermediate-weight nuclei at energies below the Coulomb barrier have been interpreted in terms of optical-model potentials, the results have had virtually no impact on present-day concepts of the potential. Several groups[9-12] have reported the $3s$ size resonance near $A = 70$. This observation is in qualitative agreement[12] with the predictions from the potential which Perey[17] obtained from an analysis of 9- to 22-MeV data. Elwyn, Marinov, and Schiffer[16] found evidence for the $3p$ size resonance which was predicted near $A = 105$. They also found a systematic ~20% disagreement with the predictions near $A = 150$, which they attributed to deformation effects. Although there are a few such deviations, these various measurements generally agree to within the experimental uncertainties with the predictions from potentials that were derived from data on $d\sigma(\theta)$ and $P(\theta)$ at higher energies. Such simple predictions are found to be inadequate in the present work which has been done with uncertainties of less than ±5%.

We chose to study the Sn isotopes because they, having a magic number of 50 protons, are not easily deformed. The deformation constants[18] are small and nearly constant ($\beta \simeq 0.11$) for the even isotopes and probably are similar for the odd ones. Thus, we avoided the large distortion effects which are expected[17] to influence the potential at low energies. We have also included work on natural In, which is mostly ^{115}In; these measurements suggest that the potential which is found for the Sn isotopes has to be modified for more deformed nuclei. Our preliminary analysis of unpublished[19] work shows that the modification increases for the deformable nuclei near $A \simeq 105$.

II. MEASUREMENTS

A. Procedures

We measured the neutrons from the (p,n) reactions in a 4π geometry with Macklin's[20] detector, a 1.5-m graphite sphere with eight BF_3 counters imbedded near its surface. Neutrons produced at the center of the sphere are thermalized in the graphite and counted at the surface with an efficiency which is nearly independent of the original energy and direction of the neutrons. Sheets of cadmium cover the surface to reduce the background from neutrons in the room. Macklin[20] found from age-diffusion theory that this detector's response is constant to better than 1% for neutron energies from a few keV to at least 1 MeV, a region that includes the calibration energy. From 1 to 5 MeV the efficiency drops about 7% due to fast-neutron leakage. Obviously, this drop-off causes no error whenever the proton energy is no more than 1 MeV above the target's (p,n) threshold. Even at higher energies the correction is negligible, because the neutrons are emitted in an evaporation spectrum which peaks at about 0.5 MeV and has relatively few high-energy neutrons. For example, for ^{115}In, which yields the highest-energy neutrons in this work, the loss calculated from the spectrum observed[21] at a proton energy of 5.3 MeV is 0.6%. The loss is less for the other targets, all of which have higher thresholds. We have neglected the correction in all cases.

We measured the detector's absolute efficiency to ±3% for 0.5-MeV neutrons by replacing the target with a Ra-Be photoneutron source whose strength ($2.58 \times 10^5 \pm 3\%$ neutron/sec) was established[22,23] by comparison with the NBS standard Ra-Be-II ($1.186 \times 10^6 \pm 3\%$ neutron sec). We then recalibrated in terms of a Pu-Be substandard for use in subsequent daily checks on the system. Eight months later we repeated this calibration of the substandard and found the same constant to within 0.3%. Corrections totaling about 2% of the observed counts were made for the background from the room, for the absorption in the target holder, and for the detector's deadtime of 9.3 ± 1.0 μsec. In the subsequent measurements of the (p,n) yields, the corrections of the same type were usually less than 3%. These corrections have negligible uncertainties.

Protons were accelerated by the 5.5-MV Van de Graaff at Oak Ridge and analyzed by a 90° magnet, which we calibrated by use of the known[24,25] (p,n) thresholds for ^{3}H, ^{7}Li, and ^{19}F. Our experience has shown that energies can be reproduced to ±0.05%; we assign an absolute uncertainty of ±0.1%. The beam diverged slowly from its small crossover near the magnet, entered through a hole in a concrete wall into a shielded room, passed through a 1.1-cm defining aperture at 5.2 m from the crossover, and formed a uniform 1.3-cm spot on the target 0.9 m beyond the aperture. We cut the aperture from 0.004-in. Pt and cleaned it to minimize backgrounds from (p,n) reactions in low-Z contaminants. We placed another aperture just before the shield wall to prevent most of the extraneous beam from reaching the main aperture.

A 75-cm-long tube positioned the target at the center of the graphite sphere and also served as a Faraday cup. A potential on the aperture suppressed secondary electron emission into the cup. We measured the charge collected to ±0.5% with a current integrator which we calibrated by placing a precision voltage across it and ten 100-MΩ ±1% resistors in series.

Table I lists the targets and some of their properties. We made the natural targets and obtained the enriched ones from the Isotopes Division at

Oak Ridge. Each target was prepared by evaporation of the metal onto a disk of 0.01-in. Pt, which was mounted directly behind a circular aperture of known area. The deposited metal was weighed to ±20 μg on a microbalance. To minimize the effects of possible target nonuniformities, we chose a target diameter, nominally 1.6 cm, so that the 1.3-cm proton beam spot would cover a large fraction of the target without danger of missing it. For the two thinner targets of ^{117}Sn and ^{119}Sn we doubled the area in order to give total deposits that could be weighed more accurately. For those two the uncertainty in the effective areal density was ±2%; for the other targets it was about ±1%. (The uncertainties were larger for the targets used in experiment 1.)

In Table I reference is made to experiments 1, 2, and 3, which we performed over a two-year period. A review of these will demonstrate some of the problems encountered. Experiment 1 proved to be preliminary, and only the results for ^{117}Sn have been normalized to the data of the latter experiments and included here. In this experiment we had some uncertainties in the current integration and in the areal densities of the targets, but our main mistake was in evaporating the targets onto Pt backings that were reclaimed from earlier work.[26] Traces of low-Z materials in some backings gave appreciable neutron yields at lower energies. For experiment 2, which gave us most of our results, we used new Pt backings which were cleaned by scrubbing with an eraser, washing with solvents and flaming to red heat. The surfaces of these Pt backings had traces of boron, which we detected by the ^{11}B(p,n) yield, a broad bump extending from the threshold[27] at 3.02 MeV to about 4 MeV on an otherwise smooth Pt background. Fortunately the yields were small and consistent so that we were able to make corrections. For experiment 3, which was done mostly for accurate measurements of atomic stopping powers,[28] we used other Pt backings and observed very few neutrons from ^{11}B(p,n). In all cases we made background corrections by use of the observed yields from duplicate backings, taking due account of the fact that the protons lose energy in the target before entering the Pt. Typically the corrections were about 10% at 2.5 MeV but decreased to 1% at 5.5 MeV. The uncertainties in the corrections have been combined in quadrature with the counting statistics and included in the error bars in the figures.

Contaminants must be minimized in the target deposit as well as in the backings. Even though care was taken to evaporate high-purity targets, there were some low-Z contaminants that gave appreciable yields below 3 MeV. Two common contaminants, with their (p,n) thresholds,[27] are ^{37}Cl (1.65 MeV) and ^{65}Cu (2.17 MeV). We have discussed ^{37}Cl in an earlier report[28]; fortunately its threshold yield is easily recognized and its subtraction is straightforward. Copper is a common impurity in separated isotopes because Cu containers are used in the separation process. We had the enriched targets chemically analyzed for Cu after the experiment and made corrections by use of the Cu(p,n) excitation function from an auxiliary measurement. The estimated uncertainties in these corrections are included in the error bars in the figures. Some of the targets may have had other unidentified low-Z contaminants; for this reason the measurements below 3 MeV have been mostly ignored in the discussions of the later sections.

We also measured the excitation function for normal Sn in order to provide cross-checks on the

TABLE I. The targets studied and some of their properties.

Target	(p,n) reaction Q value (keV)	Experiment	Isotopic purity (%)	Areal density (mg/cm^2)	Thickness at 4.5 MeV (keV)
^{117}Sn	2525[a]	1	89.2	5.28	199
		2	89.2	0.256	10
^{119}Sn	1369[a]	2	89.8	4.82	179
		2	89.8	0.261	10
^{120}Sn	3465[b]	2	98.4	3.39	125
^{122}Sn	2405[c]	2	88.2	3.39	123
^{124}Sn	1436[c]	2	96.0	3.52	125
Sn		2		2.83	105
		3		3.96	147
In	293, 1805[c]	2		3.74	142
		3		3.91	148

[a]See Ref. 59. [b]This report. [c]See Ref. 27.

uniformities of the enriched targets and on the corrections for contaminants. Pure and uniform normal targets are easier to make than enriched ones because there are no limitations on the available metal. Hence, the supplier or chemist can deliver purer metal, an excess can be placed on the filament for the evaporation, target uniformity can be ensured by placing the target far from the filament and extra targets can be made economically for use in repeat experiments. As expected, the excitation functions for normal Sn and In showed no signs of contaminants, and the reproducibility of the excitation functions for different targets was excellent.

In the following tables and figures each $\sigma_{p,n}$ is listed or plotted at a discrete proton energy E_{AV}; whereas, the observed cross section $\bar{\sigma}_{p,n}$ was an average over the proton energy loss ΔE in the target. Because of the strong energy dependence, the assignment of $\sigma_{p,n}$ and E_{AV} is not trivial. By use of accurate (±0.3%) atomic stopping powers[28,29] we calculated ΔE with negligible uncertainty for the given areal densities and assigned E_{AV} equal to the average energy in the target. However, $\sigma_{p,n}$ is not quite $\bar{\sigma}_{p,n}$. If the excitation function rises rapidly and smoothly within the interval ΔE, as it does over larger intervals, then $\bar{\sigma}_{p,n}$ is slightly greater than would have been observed with good resolution at E_{AV}. To obtain correction factors we first fit the expression $\alpha e^{\beta/E}$ to the excitation function and then integrated over ΔE. The β was chosen by successive approximations to fit the shape of the final excitation function. Typical corrections were –5% for a 200-keV target at 2.7 MeV, –2% at 3.2 MeV, and much less at higher energies. We emphasize that this conversion of $\bar{\sigma}_{p,n}$ to $\sigma_{p,n}$, and the associated assumption of a smooth behavior, is a matter of convenience rather than necessity. An equivalent procedure would have been to report the observed averages and then make comparisons with theoretical values averaged over the same ΔE's, but that would have required more optical-model calculations.

The strong energy dependence made it imperative to measure the proton energies carefully. As stated above, the estimated systematic uncertainty in the proton energies is ±0.1%. This can be transformed into an uncertainty in cross section by use of the empirical excitation function, $\alpha e^{\beta/E}$ Typical results are ±1.3% at 3 MeV and ±0.7% at 5.5 MeV. Additional random uncertainties of about half of these values arise from fluctuations in the energy settings.

An error in the areal density of a target propagates in similar manner through ΔE to a cross section, but this effect happens to cancel about half of the correlated error which is introduced directly into the cross section. Thus, errors in weights or areas for the thicker targets cause smaller uncertainties than might have been expected.

B. Cross Sections

We measured $\sigma_{p,n}$ for normal Sn and In during experiments 2 and 3. Table II lists the results from Exp. 3, which was the better of the two. We have plotted ratios of these cross sections to a smooth curve through the observed ^{124}Sn excitation function; this a convenient linear plot which displays small details. Table III lists the smooth values at 250-keV intervals; values in parentheses are extrapolations beyond the data. Interpolations can be made by use of the empirical function $\alpha e^{\beta/E}$. Figure 1 shows the ratios for both Exp. 2 and 3. The chance that there might be systematic errors in these two experiments is reduced by the fact that they agree to better than 1%, even though they

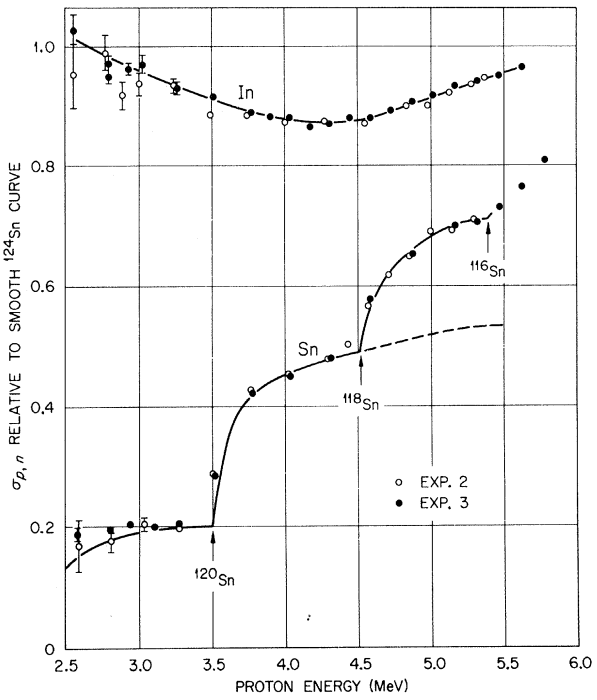

FIG. 1. The (p,n) cross sections of normal Sn and In relative to a smooth ^{124}Sn curve (see Table III). The two symbols represent two experiments which were performed about two years apart and almost independently of each other. Threshold energies from Table I or from Ref. 27 are indicated for ^{116,118,120}Sn. For Sn the solid curve below the ^{118}Sn threshold and the dashed curve above were calculated from a weighted sum of the isotopic curves in Fig. 2. The solid curve above the ^{118}Sn threshold and the In curve were drawn visually to fit the points.

TABLE II. The (p,n) cross section of In and Sn from experiment 3.

E (keV)	σ for In (mb)	σ for Sn (mb)
2581	0.0119	0.0022
2803	0.035	0.0072
2941	0.066	0.0141
3034	0.100	...
3106	...	0.0279
3273	0.248	0.0547
3520	0.578	0.180
3776	1.24	0.589
3907	1.78	...
4039	2.53	1.29
4174	3.48	...
4311	4.82	2.66
4450	6.61	...
4590	8.79	5.79
4733	11.68	...
4878	15.42	11.07
5025	19.8	...
5174	25.4	19.1
5325	31.9	24.0
5478	39.5	30.5
5633	48.8	38.8
5791	...	49.6

were performed nearly two years apart and almost independently of each other.

The cross sections for the isotopes of Sn are presented in Table IV and Fig. 2. We observed the ^{120}Sn threshold at 3494 ± 7 keV corresponding to $Q = -3465 \pm 7$ keV. Data points in the figure differ from those in the table by a few additions and omissions which are explained below. The corrections for counter deadtime, neutron backgrounds, and energy averaging effects were discussed above. In addition corrections have been made for the yields from the less abundant Sn isotopes by use of excitation functions which are consistent with the final ones. Measurements for the two thin targets were taken only near the analog-state resonances in ^{117}Sn and ^{119}Sn and have been published elsewhere,[30] but they are also plotted here at off-resonance energies. The letters A in the figure indicate energies where the on-resonance data have been omitted. The near-resonance data from the thick targets are not plotted but are included in the table. All of the cross sections were measured in Exp. 2 except for the ^{118}Sn cross sections and the ^{117}Sn values that are listed in the table. We now discuss these two exceptions.

TABLE III. Smooth curve for the (p,n) cross sections for ^{124}Sn. Values above 5.5 MeV are extrapolations beyond the measurements. Interpolation between points can be made by plotting $\ln\sigma$ versus E^{-1}.

E (MeV)	σ (mb)	E (MeV)	σ (mb)
2.50	0.0073	4.50	8.34
2.75	0.028	4.75	13.49
3.00	0.089	5.00	20.71
3.25	0.244	5.25	30.43
3.50	0.591	5.50	42.75
3.75	1.292	5.75	(58.32)
4.00	2.588	6.00	(77.29)
4.25	4.810		

TABLE IV. The (p,n) cross sections of isotopes of Sn.

^{117}Sn		^{119}Sn		^{120}Sn		^{122}Sn		^{124}Sn	
E (keV)	σ (mb)	E (keV)	σ (mb)	E (keV)	σ (mb)	E (keV)	σ (mb)	E (keV)	σ (mb)
2965	0.032	2989	0.059	3630	0.47	3029	0.091	3024	0.099
3203	0.095	3107	0.093	3758	0.87	3265	0.236	3141	0.158
3449	0.26	3227	0.157	3887	1.37	3511	0.54	3260	0.260
3702	0.64	3349	0.238	4019	2.05	3764	1.20	3381	0.392
3964	1.41	3473	0.369	4152	2.92	4025	2.42	3505	0.60
4098	2.05	3599	0.555	4287	4.18	4295	4.89	3630	0.91
4234	2.92	3727	0.82	4425	5.66	4432	6.68	3757	1.34
4371	4.35	3857	1.19	4564	7.81	4572	8.94	3887	1.89
4455	6.00	3989	1.71	4706	10.3	4713	11.8	4018	2.71
4511	6.53	4123	2.44	4849	13.6	4799	13.9	4152	3.80
4568	7.35	4259	3.45	4995	18.1	4856	15.5	4287	5.28
4653	8.1	4397	4.99	5142	23.3	5002	19.9	4425	7.12
4797	10.3	4537	7.00	5292	29.5	5091	22.9	4564	9.54
4942	13.8	4679	9.85			5150	25.1	4706	12.5
5090	18.0	4823	12.7	^{118}Sn				4849	15.9
5240	22.5	4969	16.1	4591	3.6			4995	20.6
5392	28.2	5117	20.8	4879	10.1			5142	26.0
				5175	19.8			5292	32.4
				5326	24.6			5352	35.2

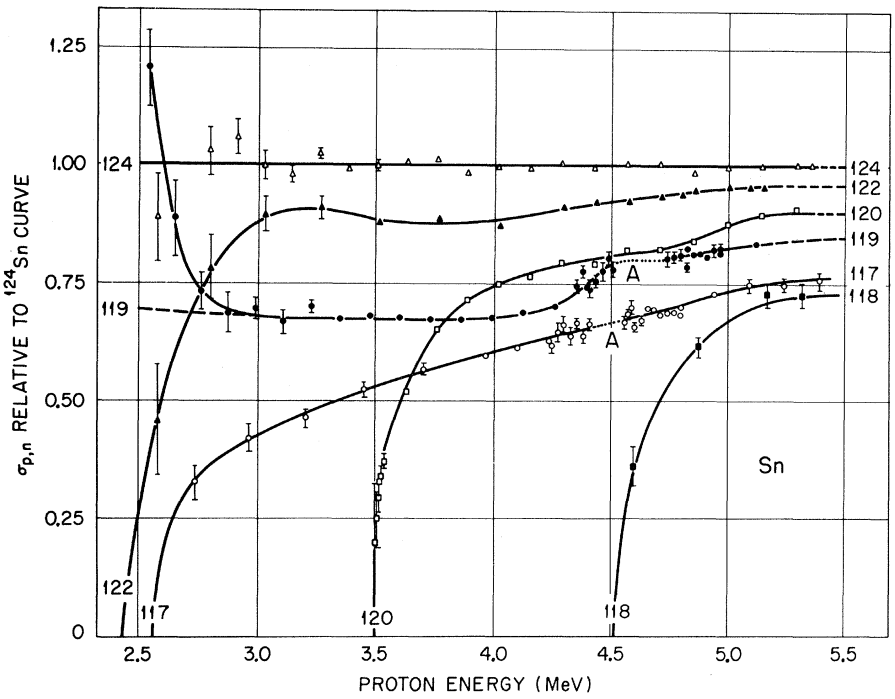

FIG. 2. The (p,n) cross sections of the Sn isotopes relative to a smooth ^{124}Sn curve (see Table III). The solid curves were drawn visually to fit the points and to vanish at the thresholds. Points near the analog-state resonances for ^{117,119}Sn are from Ref. 30; the letter A indicates energies where the resonance data are omitted. For ^{119}Sn the anomalous behavior below 3 MeV is attributed to a low-Z contaminant, and the dashed curve is probably nearer to the true excitation function.

Data for the thicker ^{117}Sn target in Exp. 2 had to be discarded because the target had an oily appearance and gave inconsistent cross sections. The values in the table and those away from the resonance in the figure were obtained from the preliminary measurements, Exp. 1, and were normalized by a factor of 1.065 to agree with the off-resonance data for the thinner target in Exp. 2. The uncertainty in the normalization is about ±2%. The good agreement between the thick- and thin-target data from Exp. 2 for ^{119}Sn is a good indication that the normalization is valid. Furthermore, comparisons of the results for ^{120,122,124}Sn from the two experiments showed good agreement, except at low energies, in the shapes of the excitation functions, and indicated that the normalization factors for these three isotopes would have been about the same as that used for ^{117}Sn. (Results from the ^{119}Sn target in Exp. 1 were useless; the target had a serious contaminant.)

As indicated above, we included measurements on normal Sn as a cross-check on the weighted sum of the isotopic excitation functions. Thereby, we also obtained the ^{118}Sn cross sections. In Fig. 2 the solid curves, excepting ^{118}Sn, are drawn visually to fit the excitation functions and to vanish at the thresholds corresponding to the Q values in Table I. The anomalous behavior for ^{119}Sn below 3 MeV probably comes from an unknown low-Z contaminant, and the dashed curve is nearer to the true excitation function. We constructed a curve for normal Sn (excluding ^{118}Sn) from a weighted sum of the isotopic curves, with reasonable assumptions for the rare ^{115}Sn isotope and with the dashed curve for ^{119}Sn. Returning to Fig. 1, we show this sum curve, solid below the ^{118}Sn threshold[27] and dashed above. Subtraction of the dashed curve from the data points yields the ^{118}Sn cross sections that were presented in Table IV and Fig. 2.

The sum curve and the data points for normal Sn in Fig. 1 agree to about 1% for energies above 3.2 MeV except, as expected, near the thresholds. Below 3.2 MeV the curve falls below the points, indicating either that the normal Sn was contaminated or that some of the isotopic excitation functions were overcorrected. As a result of this comparison, as well as the anomalous behavior of ^{119}Sn, we assign uncertainties due to unknown contaminants of ±25% at 2.5 MeV, ±5% at 3 MeV and much less above 3.5 MeV. The rapid decrease in the uncertainties is due to the fact that the Sn excitation functions rise much faster with energy than do the functions for low-Z materials.[28] We have omitted points below ~3 MeV from Table IV.

TABLE V. Uncertainties in the cross sections. The uncertainty for the primary neutron source is the quoted standard deviation; the others are estimated standard deviations as discussed in the text.

Systematic	
Primary neutron source	±3%
Relative source calibration	±0.2%
Current integration	±0.5%
Fast-neutron leakage	<0.6%
Propagation of energy uncertainty	±1.3% at 3 MeV
	±0.7% at 5.5 MeV
Total systematic	±4%
Relative and random[a]	
Random energy settings	±0.7%
Areal densities	±0.7% (^{117}Sn, ±2%)
Target contaminants[b]	±5% at 3.0 MeV
	±2% at 3.5 MeV
	<±1%, E > 4.0 MeV

[a]Additional random uncertainties arising from counting statistics and background subtraction are indicated by the error bars in the figures.

[b]Negligible contaminants estimated in natural Sn and In.

Table V presents a summary of the uncertainties that have been discussed above. The total systematic uncertainty is ±4%. The relative values depend on the particular isotope and energy but they are generally much less than ±4%. Qualitatively, we have a lot of confidence in the excitation functions for ^{120,122,124}Sn and especially for In. We have less confidence in the functions for ^{117,119}Sn.

IV. DISCUSSION AND ANALYSES

In Fig. 2 the excitation functions for the Sn isotopes show a simple A dependence perturbed only by the presence of thresholds and analog-state resonances. Probably the ^{118}Sn function, at an energy a little further above its threshold, will be situated between ^{117}Sn and ^{119}Sn. Although any complex potential would predict a systematic A dependence, it seems surprising that such predictions may be literally true rather than just on the average. These functions are good candidates for an optical-model analysis. We will make a qualitative analysis before obtaining a specific least-squares fit.

A. Definition of the Average Strength Function

The dominant feature of the (p,n) excitation functions is the strong energy dependence which arises from the external Coulomb field. It is desirable to factor out this energy dependence in order to facilitate comparisons between theory and experiment. Actually we have already removed most of the energy dependence in the above figures but we desire to do it in a different manner that will more clearly reveal the nuclear effects. This is the role of the average strength function.[9-11,16,21]

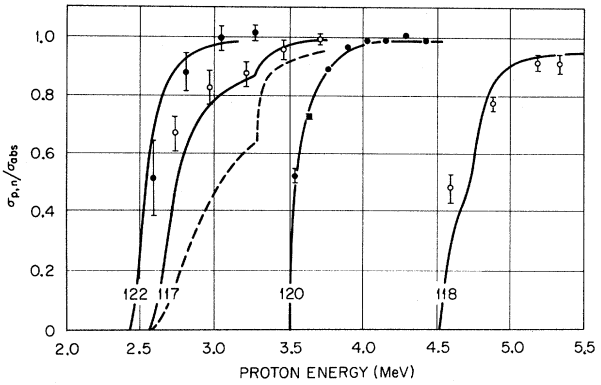

FIG. 3. Hauser-Feshbach statistical-model calculations of $\sigma_{p,n}/\sigma_{abs}$ near the ^{117,118,120,122}Sn thresholds. The purpose of the calculations was to determine energies where $\sigma_{p,n} \cong \sigma_{abs}$. Solid curves were found for arbitrary but reasonable assumptions for γ-ray emission; the dashed curve represents a poor choice for the radiative strength. Data points were obtained from Fig. 2 on the basis of assumed well-behaved curves for σ_{abs}.

The absorption cross section, averaged over many resonances, can be written[5]

$$\sigma_{abs} = \pi k^{-2} \sum_{Jsl} g_J T_{slJ} \,, \qquad (1)$$

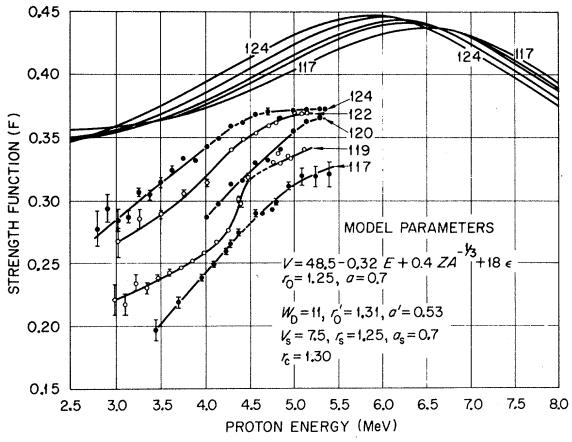

FIG. 4. Average strength functions for isotopes of Sn. Cross sections from Fig. 2 have been converted to $\overline{S}$ for energies where $\sigma_{p,n} \cong \sigma_{abs}$. Groups of points near the analog-state resonances in Fig. 2 have been averaged and plotted as single points here. The curves through the points were drawn visually. The family of curves in the upper part of the figure were calculated with the listed model parameters. This model is the same as used to fit elastic scattering at 9.8 MeV (see Refs. 34 and 37) except for the increase in V which results from the dependence, $-0.32E$, on proton energy.

where the transmission factor T_{slJ} is the difference between unity and the absolute square of the average diagonal component of the collision matrix, the sum is over orbital and total angular momentum and channel spin, and g_J is a statistical spin factor. When a proton optical-model potential is assumed, the transmission factors can be calculated. For a model including a spin-orbit potential, Eq. (1) reduces to[5]

$$\sigma_{\text{abs}} = \pi k^{-2} \sum_l \left[l T_{lj^-} + (l+1) T_{lj^+} \right], \tag{2}$$

where $j^{\pm} = l \pm \frac{1}{2}$. At energies where the transmission factors are much smaller than unity, as they are for proton energies below the Coulomb barrier, they can be approximated by[5]

$$T_{lj^{\pm}} = 4\pi f P_l s_{lj^{\pm}}, \tag{3}$$

where f is a surface reflection factor, P_l is the usual square-well penetration factor kR/A_l^2, and s_{lj^+} and s_{lj^-} are nuclear strength functions. The penetration factors increase rapidly with energy; whereas, the strength functions vary slowly and exhibit broad size resonances near the virtual single-particle states of the potential. The cross section can then be written as a weighted sum of strength functions;

$$\sigma_{\text{abs}} / \pi k^{-2} = \sum_l w_l s_l, \tag{4}$$

where

$$w_l \equiv 4\pi (2l+1) f P_l$$

and

$$(2l+1) s_l \equiv l s_{lj^-} + (l+1) s_{lj^+}.$$

A reasonable definition of an average strength function is then

$$\bar{S} = R \frac{\sigma_{\text{abs}}}{\pi k^{-2} \sum_l w_l} \equiv \frac{\sigma_{\text{abs}}}{4\pi^2 k^{-1} \sum_l (2l+1) f A_l^{-2}}, \tag{5}$$

where the radius R has been inserted to maintain conformity with the definition which has often been used in the literature.[10, 11, 16, 21]

The magnitude of $\bar{S}$ depends partly on the reflection factor f, which increases with the surface thickness. Vogt[31] has shown that when f is chosen appropriately for the surface thickness, the total single-particle reduced width obtained by integrating s_{lj} over the size resonance is approximately the sum-rule limit $\hbar^2/MR^2$. For the present work an approximation which gives integrated reduced widths of about $\hbar^2/MR^2$ is to replace fP_l at the nuclear surface by P_l at about 1 F outside of the surface. Specifically, we will compute both theoretical and experimental values of $\bar{S}$ from Eq. (5) with $f = 1$ and with A_l^2 evaluated at $R = 1.45A^{1/3}$. Since the same procedure has been used by others,[10,11,16,21] our experimental strength function can be compared directly with theirs.

Some parenthetical remarks are appropriate. We feel that this definition of $\bar{S}$ is a good one, but some might feel that another definition would be better. Actually, the chosen definition is not very important. It can be regarded as a vehicle for the comparison of the experimental cross sections to the predictions of an optical model. Once a model is chosen to fit the data, it should be intrepreted in terms of the strength functions of the various partial waves rather than in terms of the average. Another rather subtle point is that our procedure of calculating the experimental strength functions at the outset and then making comparisons with predictions from various models is not fully consistent with the concept for a reflection factor because, with this procedure, a change in the assumed surface thickness for a model changes the theoretical $\bar{S}$ rather than f. This is only an inconsistency in the visual search procedure rather than in the final interpretation.

B. Experimental $\bar{S}$ for the Sn Isotopes

Experimental strength functions can be derived from the observed (p, n) cross sections if neutron emission dominates, i.e., if $\sigma_{p,n} \simeq \sigma_{\text{abs}}$. This approximation is expected to be good at proton energies far enough above threshold such that many neutron channels are open. Thus, it is expected to be good for ^{119}Sn and ^{124}Sn, which have thresholds far below our region of interest, but it is not valid for the other isotopes near their thresholds, which are all within or not far below our region of interest.

We used the Hauser-Feshbach[32] statistical theory to estimate the minimum energies above which neutron emission dominates. Figure 3 shows the results of these calculations, which are discussed in the Appendix. Competition from γ-ray emission is important near the thresholds. The dashed curve is a poor fit to our data that was obtained with a poor choice of the radiative strength, and the solid curves are fairly good fits obtained with appropriate radiative strengths. Proton emission is completely negligible for all except ^{118}Sn, the nucleus with the highest threshold; hence, all of the curves except that for ^{118}Sn rise above 99% and approach unity within our region of interest. For ^{118}Sn the predicted proton emission accounts for the fact that the excitation function falls below rather than above ^{117}Sn; this effect provides a good check on the Hauser-Feshbach calculations. Although several parameters entered into these calculations the results do show the regions where

$\sigma_{p,n} \simeq \sigma_{abs}$. The same conclusions would have been reached with other sets of reasonable parameters providing they also described the data near the thresholds.

Figure 4 presents the experimental strength functions which have been determined from Eq. (5) with the aid of a computer program[33] for calculating the Coulomb functions. Points have been included only if $\sigma_{p,n}/\sigma_{abs} > 97.5\%$ on the Hauser-Feshbach curves of Fig. 3, and the first few points above each cutoff energy have been corrected by small amounts by reference to Fig. 3. Some of the points near the analog-state resonances have been averaged and plotted as single points.

A few comparisons can be made to other work. Elwyn, Marinov, and Schiffer[16] found $\bar{S} = 0.373 \pm 0.030$ F for normal Sn for 6.5- to 7.0-MeV protons; this is a consistent extrapolation in the figure. (We have divided their published value by 2 to agree with our definition of $\bar{S}$.) Schiffer and Lee[10] found 0.438 ± 0.06 F for 3.5- to 4-MeV protons, in disagreement with our results. For 5.3-MeV protons, Bramblett and Bonner[21] found 0.42 ± 0.04 F for ^{120}Sn and 0.53 ± 0.05 F for ^{122}Sn; the first of these is consistent with ours, but the second is not.

C. Optical-Model Potential

To be consistent with the analyses of the elastic scattering[34,35] from the Sn isotopes at higher energies, we used the conventional model that was used there, i.e.,

$$V(r) = -Vf(x) + i4W_D \frac{d}{dx'} f(x') + V_{so} \frac{\vec{\sigma}\cdot\vec{l}}{r}\left(\frac{\hbar}{m_\pi c}\right)^2 \frac{d}{dr} f(x_{so}) + V_C , \quad (6)$$

where

$$f(x) = (e^x + 1)^{-1}, \quad x = (r - r_0 A^{1/3})/a,$$
$$x' = (r - r_0' A^{1/3})/a',$$

and

$$x_{so} = (r - r_{so} A^{1/3})/a_{so} .$$

The real part is the sum of the Woods-Saxon well, a Thomas-type spin-orbit term and a Coulomb potential V_C for a uniformly charged sphere of radius $r_C A^{1/3}$. The imaginary absorptive term is peaked at the surface. The dependence of the real well depth on energy, charge and mass is often written[17]

$$V = V_0 - b_0 E + 0.4Z/A^{1/3} + V_1 \epsilon , \quad (7)$$

where $\epsilon = (N - Z)/A$. The asymmetry term $V_1\epsilon$ is attributed[36] to an isospin dependence; both the energy dependence and the Coulomb correction are expected because of the velocity dependence (nonlocality) of the potential. The particular estimate,[17] $0.4Z/A^{1/3}$, for the Coulomb correction is from a velocity dependence that would give $b_0 = 0.3$ MeV^{-1}.

D. Qualitative Optical-Model Search

The parameters should be chosen consistently with those from elastic-scattering data at higher energies. Thus, for our initial step, we calculated theoretical strength functions simply by extrapolating from the analyses[34,37] of $d\sigma(\theta)$ for 9.8-MeV protons on ^{116,120,124}Sn under the assumption that only V is energy dependent, with $b_0 = 0.32$ MeV^{-1}. Becchetti and Greenlees[38] obtained this b_0 from a comprehensive survey of experiments, and Perey[39] found this value specifically for ^{120}Sn from data above 14 MeV. As stated below, this coefficient is consistent with the potentials[34,35,37] for 9.8- to 16-MeV protons on the Sn isotopes. Transmission factors were calculated with Smith's[40] subroutine TLJ. For $E \geq 2.5$ MeV these factors agree[41] to within 0.2% with those from other independent codes at Oak Ridge. Figure 4 and model A of Table VI show the predicted strength functions and the corresponding parameters. These curves disagree with the data principally in that they show too little isotopic dependence and too high strength functions, but they provide a good starting point.

We then plotted many theoretical curves in order to see the effects of the various parameters in the potential. The following discussion is based on this survey and is made within the context of Eq. (6). We did not vary the spin-orbit potential because it is rather well established and not critical here.

TABLE VI. Optical-model parameters for Sn. (Values adjusted by least squares are in parentheses.)

Parameter	Model			
	A	B	C	D
V_0	48.5	58.4[a]	58.8[a]	58.0[a]
b_0	0.32	(0.88)	(0.92)	(0.84)
V_1	18.0	24.0	24.0	24.0
r_0	1.25	1.2	1.2	1.2
a	0.7	(0.60)	0.7	0.7
W_D	11.0	(6.0)	(11.4)	(9.44)[b]
r_0'	1.31	1.31	(1.31)	1.31
a'	0.53	0.53	(0.24)	$(0.093 + 0.052E)$[b]
V_{so}	7.5	6.0	6.0	6.0
r_{so}	1.25	1.1	1.1	1.1
a_{so}	0.7	0.7	0.7	0.7
r_C	1.3	1.21	1.21	1.21
χ^2		26	12	7

[a] $V_0 = 49.6 + 10b_0$.

[b] Fit required $W_D a' = 5.83$ MeV F for 10-MeV protons.

The most distinctive feature of each curve is a broad peak which results from a resonance in p waves. The energy for this $3p$ size resonance is determined primarily by the "volume" VR^2 of the potential. This effect is related to a well-known feature at higher energies; there the positions of peaks and valleys in scattering distributions are determined by VR^n with $n \simeq 2$. In Fig. 4 the progressive shift of the resonance as A increases from 117 to 124 is due to the increase in both R, as $A^{1/3}$, and in V, as $V_1\epsilon$.

The best fit is obtained when VR^2, or Vr_0^2, is increased in order to shift the $3p$ maximum for ^{124}Sn down to about 5 MeV where the experimental strength function for this isotope appears to have a broad maximum. This requires a larger energy coefficient b_0 in order to maintain consistency with the 9.8-MeV analysis. Although we have special confidence in the shape of the ^{124}Sn function, which was reproduced in experiments 1 and 2, our conclusion about the position of the peak would be tentative if it were not supported by the A dependence of the excitation functions. If the calculated peaks were left at the positions shown in Fig. 4, the curves would cluster at the minimum near 3 MeV; whereas, when the resonances are moved downward, the curves tend to spread apart to fit the data. In other words, the observed functions seem to be situated well up on the rising sides of their respective resonances.

With the peaks so shifted the strengths remain too large. A reduction in r_0 with constant Vr_0^2 helps a little by reducing the absorption cross sections over the entire energy region. For the least-squares analyses below, r_0 is reduced to 1.2 F. A smaller Coulomb radius r_C merely reduces the effective depth of the real well and can be compensated by an increase in V. The only remaining possibilities are to change either the parameters of the imaginary potential or the diffuseness of the real well.

The first of these possibilities, to reduce the absorption via a change in the absorptive potential, is resonable. General theoretical treatments[42] show that the Pauli exclusion principle leads to such an effect at low energies. The question arises as to which is the most appropriate variable – W_D, a' or r_0'. We gave little consideration to reducing r_0' because the radius is expected[42] to increase, if anything, at low energies. Also a least-squares fit with r_0' gave a very poor fit. A reduction in W_D tends not to reduce the over-all absorption but to narrow the size resonances by raising the peaks and lowering the valleys. This behavior is analogous to that reported by Vogt[31] and by Moldauer[43] for the neutron strength functions. A fit to the data requires not only a narrowing of the size resonances but also an over-all reduction in absorption; these are both accomplished by reducing the surface thickness parameter a'. That parameter was most useful in the following least-squares analyses.

The other possibility, to reduce the real diffuseness, may have some justification.[31] Since reflection is sensitive to the surface thickness, a small decrease in the diffuseness can produce average agreement with the experiment. However, since the main effect is to lower the curves without changing their shapes, a reduction in W_D is also needed to narrow the resonances. In one of the following least-squares fits (model B), a 15% reduction in diffuseness produces average agreement in magnitude; but a 50% reduction in W_D is also found, and the fit is not good.

E. Fixed Parameters

The foregoing study helped not only for an understanding of the problem but also for choosing the fixed and the initial variable parameters in the least-squares search. In all cases we fixed r_C, r_0, V_1, V_{so}, r_{so}, a_{so}, and $V_0 - 10b_0$ by reference to both the 9.8-MeV analyses and to the more recent analysis[35] of elastic scattering from the $^{112, 116, 118, 120, 122, 124}$Sn isotopes at 16 MeV.

The spin-orbit and Coulomb potential parameters are not critical. We chose $V_{so} = 6$ MeV, $r_{so} = 1.1$ F, and $a_{so} = 0.7$ F from the more recent work[35] at 16 MeV. The radius r_C used at 9.8 MeV was 1.3 F and at 16 MeV was 1.2 F; we used nearly the latter value, specifically 1.21 F, in accordance with data from muonic x rays and electron scattering.[44] The fact that the Coulomb radii for the Sn isotopes vary[44] less rapidly than $A^{1/3}$ has a negligible effect here. For the asymmetry potential, the qualitative survey showed that a value of V_1 larger than 18 MeV helps to fit the large isotopic dependence. Actually, this value, which was found at 9.8 MeV, is smaller than usual. Becchetti and Greenlees[38] obtained 24 MeV from their general analysis, and we found that this gives a good visual fit to the potentials for the 16-MeV data, providing ^{112}Sn is excluded from those data, as it was at 9.8 MeV. Therefore, we assumed $V_1 = 24$ MeV. Finally, we assumed $r_0 = 1.20$ F in accordance with the analysis at 16 MeV, although an even smaller radius, say 1.17 F as given by Becchetti and Greenlees, might have been useful.

Thus, we found ourselves taking most of the parameters for the real potentials from the analysis at 16 MeV rather than from the nearby energy of 9.8 MeV. Ideally we should have reanalyzed the 9.8-MeV scattering data to find a new V_0; but rather than that, we found V_0 at 9.8 MeV approximately from two independent approaches. One method

was to reexamine the published potentials at 9.8 MeV in order to find V_0 consistent with $V_1 = 24$ MeV, then to correct for the decrease in r_0 according to the Vr_0^n dependence, and finally to make a 1-MeV correction based on our calculations for the effect of the reduced r_C. The second approach was simply to use V_0 from the analysis at 16 MeV and assume $b_0 = 0.32$ MeV^{-1}, as indicated by the curve labeled "$52.8 - 0.32E$" in Fig. 5. The two methods gave the same real well depth to within 0.3 MeV. As a further check, we used this new well depth to calculate the strength functions, still assuming that $b_0 = 0.32$ MeV^{-1}, and found the peaks of the size resonance near those calculated originally in Fig. 4.

The combined constant, $V_0 - 10b_0$, remained to be chosen. Below 10 MeV ($\simeq$9.8 MeV) our survey has shown that the slope b_0 should be increased in order to shift the size resonances down in energy. We approximated this nonlinearity by a discountinuity in slope at 10 MeV. We then correlated V_0 and b_0 by fixing the potential at 10 MeV ($V_0 - 10b_0 = 49.6$ MeV) and let b_0 be the variable below 10 MeV. Figure 5 illustrates this discountinuity for one of the least-squares fits.

F. Least-Squares Analysis for the Sn Isotopes

We used Perey's[45] search routine GENOA with modifications[41] which ensure that the scattering matrix elements are calculated with sufficient accuracy, ~0.2%, down to proton energies of 2.5 MeV. GENOA has the capacity to calculate strength functions for up to 30 combinations of A, Z, and E

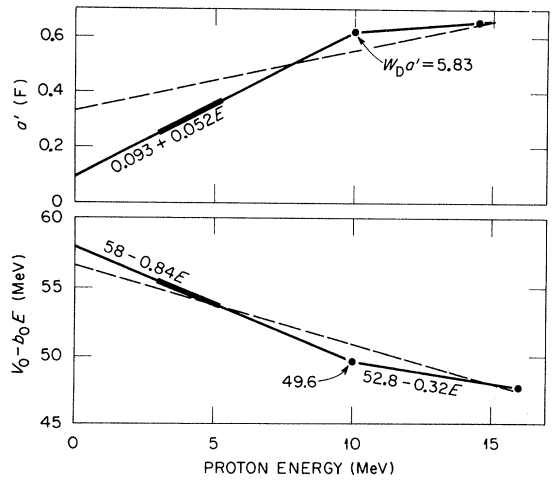

FIG. 5. Energy dependence for the real well depth and for the diffuseness a' of the imaginary potential. The solid curves below 10 MeV refer to model D for the Sn isotopes, and the intensified lines show the energy range for the present work. Data points refer to other work. The dashed curves refer to In.

and to minimize χ^2, which is defined as usual,

$$\chi^2 = \frac{1}{N} \sum_{i=i}^{N} w_i \left[1 - \frac{\bar{S}_i(\text{th})}{\bar{S}_i(\text{exp})}\right]^2 , \tag{8}$$

where

$$w_i = [\bar{S}_i(\text{exp})/\Delta\bar{S}_i]^2 .$$

Since w_i is a relative weight, $\Delta\bar{S}_i$ must be a relative uncertainty in the experimental strength function $\bar{S}_i(\text{exp})$. This does not include the ±4% absolute systematic uncertainty; furthermore, the systematic uncertainties in the individual excitation functions enter into $\Delta\bar{S}_i$ in a different manner from the random errors within an excitation function. With these complications, the reduction of the original 80 points to 30, appropriately weighted for GENOA, was not straightforward. The original points were weighted and combined in groups of 2 to 5. The resulting relative total weights for the excitation functions were nearly proportional to the energy spans covered by each excitation function, except that about half of the ^{117}Sn weight was transferred to ^{124}Sn. A visual examination of the resulting least-squares curves in relation to the original 80 points indicates that the set was well chosen. We attempted to assign appropriate random errors; nevertheless, only relative values of χ^2 are really meaningful.

We made many least-squares searches. Models B and C in Table VI show the results for two of these; a figure showing these fits was given in our earlier report.[3] The three variables were b_0 and W_D for the real and imaginary well depths and either one or the other diffuseness parameter; a for model B and a' for model C. The fixed values for a and a' are those used at 9.8 MeV. As indicated, a supplementary search showed that the assumed imaginary radius is also the best-fit value for model C. As expected, both searches found that a large energy dependence, $b_0 \simeq 0.9$ MeV^{-1}, is required in order to place the peak of the ^{124}Sn size resonance near 5 MeV. Also, as expected, the product $W_D a'$ and one of the diffuseness parameters had to be reduced from their values for 9.8-MeV protons. These latter two requirements were satisfied simultaneously in the best fit, model C, by reducing the imaginary diffuseness parameter about a factor of 2. For the poorer fit, model B, both the real diffuseness parameter and W_D were reduced.

We also made a brief search on the imaginary-potential radius r_0' rather than on a or a' and found an apparent minimum but a very poor fit with r_0' less than r_0. This seems to corroborate the conclusion from the preliminary survey that r_0' is not a very useful variable.

Our conclusion at this point was that the real well depth is somewhat deeper and the surface absorptive layer somewhat thinner than at 9.8 MeV. So both have energy dependences. We then introduced a linear dependence for a' under the restriction that the pertinent parameter, $W_D a'$, remain the same for 9.8-MeV protons, as found in the original analysis,[34] i.e., 5.83 MeV F. A search under these conditions gave model D of Table VI. This was a three-parameter search much like that of model C but the fit is better. The energy dependence for the model parameters are shown in Fig. 5.

Figure 6 shows the fit to the data for this model. In the lower figure the curves are plotted together for ease of intercomparison, and in the upper figure they are plotted again, displaced from each other for comparisons with the data. The ^{117,119}Sn analog resonances[30] are included with the data. The fits are good although there is a systematic deviation between theory and experiment for 3- to 3.5-MeV protons on ^{119}Sn; this could easily be due to a contaminant in the target as discussed above relative in Fig. 2.

For this best fit, Fig. 7 shows the relative cross sections and the partial strength functions for s-, p-, d-, and f-wave protons on ^{124}Sn. The strength function Rs_{lj} was calculated from Eq. (3), in analogy with the definition of $\bar{S}$, with $R = 1.45A^{1/3}$ F and

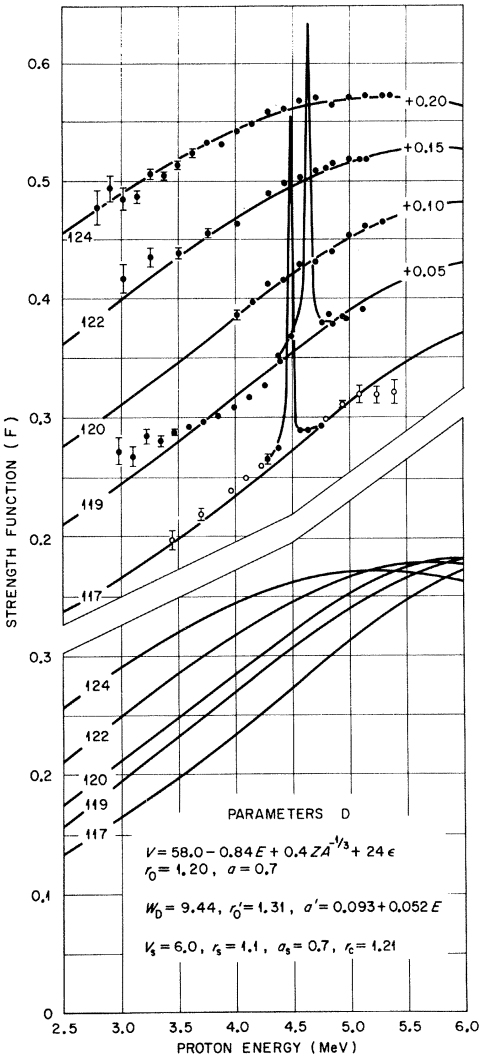

FIG. 6. Optical-model least-squares fit to the strength functions for the Sn isotopes. The family of curves of $A = 117$ to 124 in the lower figure were calculated for the listed parameters, model D. In the upper figure these curves have been reproduced, displaced from each other as indicated by the numbers at the right, for comparison with the experimental strength functions. Solid points are from experiment 2 and open points from experiment 1. Experimental curves for the analog-state resonances have been included.

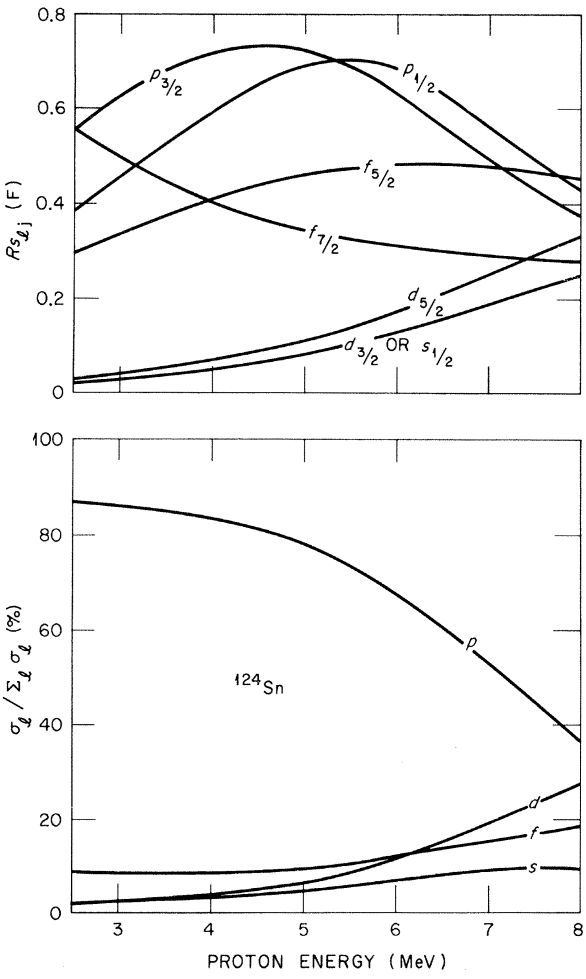

FIG. 7. Partial strength functions and relative cross sections for protons on ^{124}Sn as predicted by model D. Each strength function Rs_{lj} has been calculated from Eq. (5) in analogy with the definition of the average strength function $\bar{S}$, with $R = 1.45A^{1/3}$ F and with a reflection factor of unity.

with a reflection factor of unity. Both p and f waves exhibit resonances, which are each split by the spin-orbit potential, but the centrifugal barrier reduces the f-wave contribution to the total cross section. The p waves make up at least 75% of the total over the energy range of the experiment.

G. Absorption Cross Sections at 14.5 MeV

Clearly, it is of interest to extend these measurements to higher energies. Such work is in progress at this laboratory, but already the total absorption cross sections for protons on ^{116,117,118,119,120}Sn have been measured by Dicello, Igo, and Roush[46] at 14.5 MeV. Figure 8 shows their cross sections. The solid curve is the result of a least-squares search on the single variable a'. The other variables were all from model D except that the real well depth was taken from the line in Fig. 5 which connects the potentials for 10- and 16-MeV protons. The resulting imaginary diffuseness parameter is plotted in Fig. 5 and shows a reasonable increase from lower energies.

H. Comparison with the Neutron p-Wave Strength Functions

An intercomparison of the positions of the $3p$ size resonances for neutrons and protons is interesting. If we accept at face value the Coulomb correction and the asymmetry or isospin term, then we obtain the neutron potential by omitting the Coulomb correction and changing the sign of the isospin term. With these changes in models A (the one from 9.8-MeV scattering) and C and D (those which gave good fits to our data), we have calculated and plotted in Fig. 9 the strength functions for 200-keV neutrons on intermediate weight nuclei. The units are conventional and the experimental points are those measured by analyses of average total cross sections at Duke University.[47,48] In view of the long extrapolation from the Sn data, only a cursory discussion is warranted. The curves do confirm that the neutron well is shallower than the proton well. If it had not been made shallower by changing the sign of the asymmetry term, the peak for C or D would have been down near $A = 74$; and if the Coulomb term were also retained or incorporated into V_0, the peak would have been even lower. A possible explanation for the fact that the peaks for C and D are still about 5 mass units below the observed peak is that the Coulomb correction at low energies is larger than we have assumed; part of the increasing well depth for low-energy protons might be associated with an increasing Coulomb correction. In general, the magnitude for the curves do not agree with the experimental points. The high peak value for model D results from a very low surface diffuseness for the imaginary potential, only 0.094 F at 200 keV.

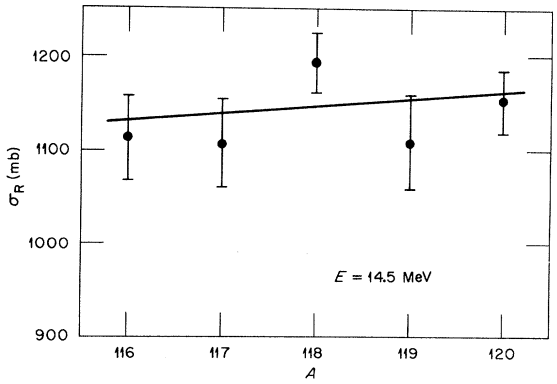

FIG. 8. The total reaction cross sections measured (see Ref. 46) for 14.5-MeV protons on isotopes of Sn. The curve is a least-squares fit obtained by adjusting a' in model D: $a' = 0.65$ F.

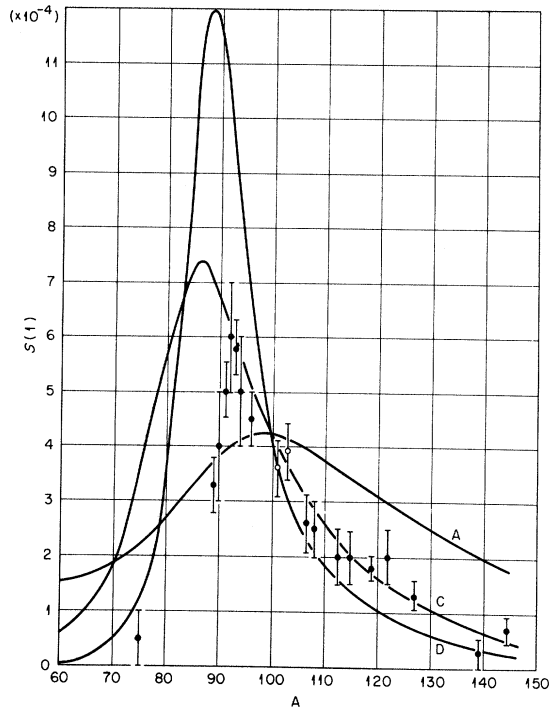

FIG. 9. Neutron p-wave strength functions. Experimental points are from Duke University, the solid points from Ref. 47 and the open circles from Ref. 48. The theoretical curves were calculated for 200-keV neutrons and then reduced to conventional units. The three curves were predicted from neutron potentials obtained from models A and C, with the specified energy dependences in the real wells, and from model D, with the energy dependence in both the real and imaginary potentials.

I. In Strength Functions

The cross sections for In are essentially those for ^{115}In, a 95.5% isotope. We have converted the cross sections from Fig. 1 into average strength functions and plotted them in Fig. 10 along with those for ^{124}Sn. The solid curve for ^{124}Sn and the dashed one for In were calculated from model D, which gave a good fit to the Sn isotopes. The resulting poor fit for In is probably related to the deformability. Perey[17] showed that the effects of greater deformability can be included in a local potential by increasing W_D, or a' and the energy dependence of V, particularly at low energies. With this in mind we began with model C and, with the parameters for 10-MeV protons still fixed, searched for and found a good fit with a' increased to 0.32 F and b_0 increased to 1.08 MeV^{-1}. This fit is not shown here. We made an unsuccessful analogous search with model D. We then changed the procedure by fixing a' and $V_0 - b_0E$ for 15-MeV protons, rather than for 10-MeV protons, and made the same type of three-parameter search as that used to find model D for the Sn isotopes. We obtained a good fit, $\chi^2 = 1.3$, as shown by the curve through the points in Fig. 10. The dashed lines in Fig. 5 indicate the new parameters; $V_0 = 56.6$, $b_0 = 0.57$, and $a' = 0.33 + 0.022E$. Also W_D has been increased to 12.26 MeV. The main effects are that both the width and the depth of the imaginary potential have been increased about 25% in order to give a broader size resonance.

V. CONCLUSIONS

At low proton energies where the (p,n) cross sections are nearly equal to the total absorption cross sections, the measured (p,n) excitation functions and the corresponding average strength functions for $^{117, 119, 120, 122, 124}$Sn show systematic A and E dependences. The following three conclusions are made within the context of a conventional proton optical potential which gives a good description of the strength functions: (1) A term in $(N-Z)$ is nesessary to fit the isotopic dependence, and the usual asymmetry term $V_1(N-Z)/A$ in the real potential is adequate with $V_1 = 24$ MeV. This term accounts for about 40% of the A dependence while the $A^{1/3}$ dependence of the radii accounts for the rest. (2) Both the E and A dependences show that the strength functions are situated near the peaks on the rising sides of p-wave size resonances. These peaks occur at lower energies than would be expected if the average energy dependence of the real well were the same below 10 MeV as it is above. To produce the size resonances at the observed energies, the real potential must have an average slope for 5- to 10-MeV protons of about three times the slope, -0.32 MeV^{-1}, observed for 10- to 16-MeV protons. (3) The over-all magnitude of the observed strength functions and the apparent widths of the size resonances are less than predicted for a potential whose diffuseness parameters and imaginary potential are appropriate for 10- to 16-MeV protons. Both discrepancies are removed when the imaginary diffuseness a' is reduced to about 0.3 F, less than half of its usual value. If this energy dependence of a' is made explicit, a slightly smaller W_D seems also to be needed. An alternative but less successful approach is to reduce both the real diffuseness and the imaginary well depth W_D. In either case the product $W_D a'$ is about half of the value found at 10 MeV.

The In strength functions (mostly ^{115}In) disagree with predictions from the best-fit potential for the Sn isotopes. The main modifications required for a particular potential which does give a good fit are increases of about 25% in both the width and the depth of the imaginary potential. These increases may be related to a greater deformability

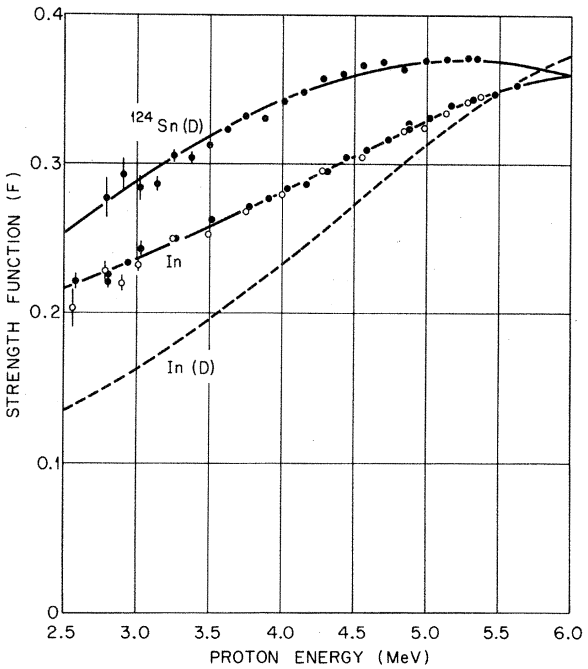

FIG. 10. Strength functions for normal In. The ^{124}Sn functions are reproduced from Fig. 6. Points for In were determined from the cross sections in Fig. 1. The curve for ^{124}Sn and the dashed curve for In were calculated from model D, the best fit for the Sn isotopes. The least-squares fit to In is for a potential that is the same as model C or D except that $W_D = 12.26$ MeV, $a' = 0.33 + 0.022E$, $V_0 = 56.6$ MeV, and $b_0 = 0.57$ MeV^{-1} (see dashed curves, Fig. 5).

for the ^{115}In nucleus.

The larger energy dependence in the real well depth at low energies was expected on both theoretical and experimental grounds. Theoretically, Slanina and McManus[49] found that the exchange term in the two-nucleon interaction has this effect. Experimentally, Fricke *et al.*[50] and Fulmer *et al.*[51] found a slope of -0.22 MeV^{-1} for 30- to 60-MeV protons and Perey[17] found about -0.44 and -0.55 MeV^{-1} for energies near 20 and 12 MeV, respectively. Perey attributed part of this increase to the effect of core excitations, but that effect is expected to be small for the Sn isotopes, which have small deformation parameters.[18]

The sharp peaking of the imaginary surface potential is more surprising, but some theoretical and experimental evidence suggests this effect. General theoretical treatments[42] show that the effects of the Pauli exclusion principle and of nuclear correlations at lower energies is to decrease the imaginary potential and to move it outward from the volume to the surface. Experimentally, rather striking similarity is found between our proton potential and the neutron potential which Moldauer[43] obtained from a survey of data on the absorption, scattering, and polarization by spherical nuclei of neutrons below 1 MeV. His potential has $a' = 0.24$ F and an imaginary radius which is 0.5 F larger than the real radius. Engelbrecht and Fiedeldey[52] took Moldauer's potential at zero energy and developed a model for 0- to 100-MeV neutrons in which the imaginary part changes continuously from purely surface absorption at zero energy to purely volume absorption at energies beyond 100 MeV. Their geometric parameters remained fixed, and in particular $a' = 0.24$ F.

A similar model for protons is appealing. Recently Perey[39] fit data for 14- to 40-MeV protons on ^{120}Sn with a model with $a' \simeq 0.7$ F in which the imaginary part changes continuously from surface to volume but in which the volume part vanishes below 14 MeV. He then found that a' must be reduced to 0.53 F for the 9.8-MeV data, in agreement with the original analysis.[34] Perhaps a model similar to that of Engelbrecht and Fiedeldey with both volume and surface absorption at all energies would avoid an energy dependence in a'.

Further measurements for other intermediate-weight nuclei at these energies and also at slightly higher energies would be quite useful for establishing an average optical-model potential for energies below the Coulomb barrier.

ACKNOWLEDGMENT

We gratefully acknowledge discussions with Dr. M. Reeves, III, Dr. F. Perey, and Dr. R. Satchler. Our analysis depended heavily on Perey's code GENOA and in particular on special adaptations which Dr. Reeves made for us. We are also grateful to members of the Isotope and Analytical Chemistry Divisions at Oak Ridge for preparation of the enriched targets and for chemical analyses after the experiment.

APPENDIX

Hauser-Feshbach Calculations

The Hauser-Feshbach[32] calculations were performed with a computer program[33] which includes the width fluctuation correction[53] for a Porter-Thomas[54] distribution of level widths. In this theory the relative probability for neutron decay of states of spin J is found by summing the optical-model neutron transmission factors over the allowed exit channels and dividing by a sum for all outgoing particles. We also included the effects[9] of γ-ray emission by adding a transmission factor T_{γ_J} to the sum for outgoing particles, where

$$T_{\gamma_J} = 2\pi\,\overline{\Gamma}_\gamma/D_J = 2\pi(2J+1)\overline{\Gamma}_\gamma/D_0 .$$

We used the radiative strength $\overline{\Gamma}_\gamma/D_0$ as an adjustable parameter to fit the yield curves near threshold and found values consistent with neutron capture data.[55,56]

For convenience, we did not modify the program specifically to include $T_{\gamma J}$ but synthesized the effect with an option which allows particle transmission factors to be fixed for specific final states. Eight fictitious final states were added with various I^π; $\frac{1}{2}^\pm$ to $\frac{7}{2}^\pm$ for odd nuclei and $0^\pm$ to $3^\pm$ for even. Transmission factors to these states were made constant; $T = T_0$ for $l \leq 2$, and zero for $l > 2$. It is then easy to show that $\overline{\Gamma}_i/D_0$ is effectively $0.75T_0$ to a good approximation.

Input parameters related to proton emission have little uncertainty. The level parameters are generally known[57] for the low-lying target states, and the optical-model parameters can be chosen so that the predicted σ_{abs} fit the data far above the threshold. Besides, proton emission turns out to be negligible except for ^{118}Sn. The probability of α-particle emission is even less and was not included in the calculations.

Neutron optical-model parameters are also known with relative certainty. In the notation of Eq. (6) we assumed $r_0 = r_0' = 1.25$ F, $a = 0.65$ F, $a' = 0.47$ F, $V \simeq 47$ MeV, $W = 11$ MeV, and $V_{so} = 0$. The details of the final states populated by neutron decay are not critical providing several states are available, as there are for the products from the even Sn targets. Some information on these odd-odd nuclei is available from Hjorth's[58] study of

(d,p) and (d,t) reactions on the Sb isotopes. He found many levels in ^{120}Sb and ^{122}Sb, some unresolved, which can be attributed to the 51st proton in possible $d_{5/2}$ or $g_{7/2}$ states coupled to the odd neutron in possible $s_{1/2}$, $d_{3/2}$, $d_{5/2}$, $g_{7/2}$, and $h_{11/2}$ states. Using his work as a guide, we assigned a large number of levels of various J^π to the nuclei ^{118,120,122}Sb. For example, we introduced 34 levels below 1.7 MeV in ^{120}Sb. In contrast, the odd-even nucleus from the ^{117}Sn$(p,n)^{117}$Sb reaction has few levels, and the parameters of the lowest ones are important. We introduced 11 levels below 1.5 MeV as determined from neutron time-of-flight measurements[59] at this laboratory.

The resulting Hauser-Feshbach curves are compared in Fig. 3 with the "observed" ratio of $\sigma_{p,n}/\sigma_{\text{abs}}$. We derived these data points from the actual $\sigma_{p,n}$ in Fig. 2 by drawing reasonable σ_{abs} curves which fit the data at higher energies and extrapolated smoothly to the energies of the thresholds. For ^{118}Sn we assumed the σ_{abs} curve lies midway between ^{117}Sn and ^{119}Sn. The theoretical curves in Fig. 3 for the even targets and the dashed curve for ^{117}Sn were calculated for $\overline{\Gamma}_\gamma/D_0 = 0.0030$; the better fitting (solid) curve for ^{117}Sn was calculated for $\overline{\Gamma}_\gamma/D_0 = 0.0004$. Both values are consistent with radiation strengths of 0.0005 to 0.003 as derived from neutron capture data[55,56] for other compound nuclei in this mass region.

---

*Research sponsored by Oak Ridge National Laboratory under contract with the Union Carbide Corporation.

†Present address: Old Dominion College, Norfolk, Virginia.

[1]G. R. Satchler, Nucl. Phys. A92, 273 (1967).
[2]P. J. Bulman and J. A. R. Griffith, Nucl. Phys. A111, 315 (1968).
[3]C. H. Johnson and R. L. Kernell, Phys. Rev. Letters 23, 20 (1969).
[4]A. R. Bodmer and J. R. Rook, Nucl. Phys. 31, 240 (1962).
[5]E. Vogt, in *Advances in Nuclear Physics*, edited by M. Baranger and E. Vogt (Plenum Press, Inc., New York, 1968), Vol. 1.
[6]T. D. Newton, Can. J. Phys. 34, 804 (1956).
[7]H. J. Kim, R. L. Robinson, and C. H. Johnson, Phys. Rev. 180, 1167 (1969).
[8]R. M. Wood, R. R. Borchers, and H. H. Barschall, Nucl. Phys. 71, 529 (1965).
[9]C. H. Johnson, A. Galonsky, and J. P. Ulrich, Phys. Rev. 109, 1243 (1958).
[10]J. P. Schiffer and L. L. Lee, Jr., Phys. Rev. 109, 2098 (1958).
[11]G. A. Jones, Nucl. Phys. 12, 167 (1959).
[12]R. D. Albert, Phys. Rev. 115, 925 (1959).
[13]H. Taketani and W. P. Alford, Phys. Rev. 125, 291 (1962).
[14]J. Wing and J. R. Huizenga, Phys. Rev. 128, 280 (1962).
[15]R. M. Humes, G. F. Dell, Jr., W. D. Ploughe, and H. J. Hausman, Phys. Rev. 130, 1522 (1963).
[16]A. J. Elwyn, A. Marinov, and J. P. Schiffer, Phys. Rev. 145, 957 (1966).
[17]F. G. Perey, Phys. Rev. 131, 745 (1963).
[18]P. H. Stelson and L. Grodzins, Nucl. Data A1, 21 (1965).
[19]C. H. Johnson, A. Galonsky, and C. H. Inskeep, Oak Ridge National Laboratory Report No. ORNL-2910, 1960 (unpublished).
[20]R. L. Macklin, Nucl. Instr. Methods 1, 335 (1957).
[21]R. L. Bramblett and T. W. Bonner, Nucl. Phys. 20, 395 (1960).
[22]J. H. Gibbons and R. L. Macklin, Phys. Rev. 114, 571 (1959).
[23]R. L. Macklin, private communication.
[24]R. O. Bondelid, J. W. Butler, C. A. Kennedy, and A. del Callar, Phys. Rev. 120, 887 (1960).
[25]J. B. Marion, Rev. Mod. Phys. 38, 660 (1966).
[26]C. H. Johnson, C. C. Trail, and A. Galonsky, Phys. Rev. 136, B1719 (1964).
[27]C. Maples, G. W. Goth, and J. Cerny, Nucl. Data A2, 429 (1966).
[28]C. H. Johnson and R. L. Kernell, Phys. Rev. 169, 974 (1968).
[29]H. H. Andersen, C. C. Hanke, H. Sørensen, and P. Vajda, Phys. Rev. 153, 338 (1967).
[30]H. J. Kim, R. L. Robinson, R. L. Kernell, and C. H. Johnson, Phys. Rev. Letters 19, 325 (1967).
[31]E. Vogt, Phys. Letters 1, 84 (1962); Rev. Mod. Phys. 34, 723 (1962).
[32]W. Hauser and H. Feshbach, Phys. Rev. 87, 366 (1952).
[33]D. Wilmore, Atomic Energy Research Establishment Report No. AERE-R5053, 1966 (unpublished).
[34]J. E. Durisch, R. R. Johnson, and N. M. Hintz, Phys. Rev. 137, B904 (1965); J. E. Durisch and P. Gould, *ibid.* 137, B906 (1965).
[35]W. Makofske, W. Savin, H. Ogata, and T. H. Kruse, Phys. Rev. 174, 1429 (1968).
[36]A. M. Lane, Nucl. Phys. 35, 676 (1962).
[37]P. C. Sood, Phys. Letters 19, 52 (1965).
[38]F. D. Becchetti, Jr., and G. W. Greenlees, Phys. Rev. 182, 1190 (1969).
[39]F. G. Perey, private communication.
[40]W. R. Smith, Oak Ridge National Laboratory Report No. TM-1234, 1965 (unpublished).
[41]M. Reeves, III, private communication.
[42]P. E. Hodgson, *The Optical Model of Elastic Scattering* (Clarendon Press, Oxford, England, 1963), p. 171.
[43]P. A. Moldauer, Nucl. Phys. 47, 65 (1963).
[44]H. R. Collard, L. R. B. Elton, and R. Hofstadter, in *Landolt-Börnstein Numerical Data and Functional Relationships in Science and Technology*, edited by K. H. Hellwege and H. Schopper (Springer-Verlag, Berlin, Germany, 1967), New Series, Group I, Vol. 2.
[45]F. G. Perey, private communication.
[46]J. F. Dicello, G. J. Igo, and M. L. Roush, Phys. Rev. 157, 1001 (1967).

[47]K. K. Seth, R. H. Tabony, E. G. Bilpuch, and H. W. Newson, Phys. Letters 13, 70 (1964).
[48]M. Divadeenam, private communication.
[49]D. Slanina and H. McManus, Nucl. Phys. A116, 271 (1968).
[50]M. P. Fricke, E. E. Gross, B. J. Morton, and A. Zucker, Phys. Rev. 156, 1207 (1967).
[51]C. B. Fulmer, J. B. Ball, A. Scott, and M. L. Whiten, Phys. Letters 24B, 505 (1967).
[52]C. A. Engelbrecht and H. Fiedeldey, Ann. Phys. (N.Y.) 42, 262 (1967).
[53]P. A. Moldauer, Phys. Rev. 135, B642 (1964).
[54]C. E. Porter and R. G. Thomas, Phys. Rev. 104, 483 (1956).
[55]L. W. Weston, K. K. Seth, E. G. Bilpuch, and H. W. Newson, Ann. Phys. (N.Y.) 10, 477 (1960).
[56]J. H. Gibbons, R. L. Macklin, P. D. Miller, and J. H. Neiler, Phys. Rev. 122, 182 (1961).
[57]*Nuclear Data Sheets*, compiled by K. Way *et al.* (Printing and Publishing Office, National Academy of Sciences – National Research Council, Washington, D.C.).
[58]S. A. Hjorth, Arkiv Fysik 33, 183 (1966).
[59]R. L. Kernell, Ph. D. thesis, University of Tennessee, 1968 (unpublished).

PHYSICAL REVIEW C VOLUME 2, NUMBER 2 AUGUST 1970

Nuclear Level Structure of ^{169}Er†

T. J. Mulligan and R. K. Sheline
Florida State University, Tallahassee, Florida 32306

and

M. E. Bunker and E. T. Jurney
University of California, Los Alamos Scientific Laboratory, Los Alamos, New Mexico 87544

(Received 24 February 1970)

Levels in ^{169}Er have been studied through the reactions ^{168}Er$(d,p)^{169}$Er and ^{170}Er$(d,t)^{169}$Er, using 12-MeV deuterons, and via thermal-neutron capture in ^{168}Er. Over 40 states below 1.5 MeV are populated in the charged-particle reactions. These data, coupled with the ≈150 capture γ rays observed, lead to a level scheme that includes the following spectroscopic assignments (rotational band-head energy in keV, followed by the Nilsson single-particle state believed to be dominant): 0.0, $\frac{1}{2}^-[521]$, with associated rotational band to spin $\frac{11}{2}^-$; 92.2, $\frac{5}{2}^-[512]$, with band to $\frac{11}{2}^-$; 243.7, $\frac{7}{2}^+[633]$, with band to $\frac{13}{2}^+$; 562.1, $\frac{1}{2}^-[510]$, with band to $\frac{7}{2}^-$; 714.5, $\frac{3}{2}^-[521]$, with band to $\frac{11}{2}^-$; 823, $\frac{7}{2}^-[514]$, with band to $\frac{9}{2}^-$; 850, $\frac{5}{2}^-[523]$, with band to $\frac{11}{2}^-$; and 1081.8, $\frac{3}{2}^-[512]$, with band to $\frac{7}{2}^-$. In addition, a level at 860.2 keV is assigned as the head of a $K^\pi = \frac{3}{2}^+$ band that is mainly the $(K-2)$ γ-vibrational state associated with $\frac{7}{2}^+[633]$. The data suggest that the 562.1-, 714.5-, and 1081.8-keV bands also have significant vibrational admixtures. Several features of the level scheme, including certain γ-ray branching ratios, are interpreted in terms of Coriolis mixing. The neutron separation energy for ^{169}Er is determined as 6003.1 ± 0.3 keV, and the Q value for the ^{170}Er$(d,t)^{169}$Er reaction is found to be −950 ± 30 keV.

I. INTRODUCTION

The nuclear energy level structure of ^{169}Er has been studied previously by several techniques. The work of Funke *et al.*[1] was concerned with the β decay of ^{169}Ho, which populates levels in ^{169}Er up to ≈0.95 MeV. The early (d,p) spectroscopic work of Isoya[2] was done with 80-keV resolution, using a target of natural Er. The (d,p) data of Harlan and Sheline[3] were obtained using an enriched ^{168}Er target; however, the enrichment was only 77%, so that the observed spectrum was complicated by the presence of numerous peaks from impurity isotopes. Recently, Bonitz,[4] from analysis of $(d,p\gamma)$ delayed-coincidence measurements, has established the existence of isomeric states at 92 and 244 keV.

In the present work, through analysis of high-resolution spectroscopic data from the reactions ^{168}Er$(d,p)^{169}$Er, ^{170}Er$(d,t)^{169}$Er, and ^{168}Er$(n,\gamma)^{169}$Er, several new energy levels of ^{169}Er have been found, and an improved understanding of a number of the established levels below 1.4 MeV has been obtained. From analysis of the charged-particle relative cross sections, along with the level energies, it has been possible to group most of the observed low-energy states into rotational bands and to deduce the Nilsson single-particle character[5] of these bands. In this analysis, the (n,γ) data have provided considerable guidance. For example, the observed primary (n,γ) transitions from the compound capture state (which has $I^\pi = \frac{1}{2}^+$) to low-lying states in the residual nucleus are almost always of dipole character, so that the *final* states can be as-